J Ther Eng, Vol. 10, No. 5, pp. 1292−1305, September, 2024

Journal of Thermal Engineering
Web page info: https://jten.yildiz.edu.tr
DOI: 10.14744/thermal.0000867

Research Article

An experimental study for a single-pass solar air heater integrated with artificial roughness

Nabaa M. BADER[1,2,*], Khudheyer S. MUSHATET[2]

[1]*College of Engineering Technology, National University of Science and Technology, Thi-Qar, 64008, Iraq*
[2]*Department of Mechanical, College of Engineering, University of Thi-Qar, Thi-Qar, 64001, Iraq*

ARTICLE INFO

Article history
Received: 28 July 2022
Revised: 07 February 2023
Accepted: 08 February 2023

Keywords:
Artificial Roughness; Friction Factor; Solar Air Heater; Thermal Efficiency

ABSTRACT

The utilization of solar air heaters are significant due to its capacity to diminish the reliance on fossil fuel-based power usage, hence mitigating pollution and conserving energy. The thermal-performance of a solar heater was analyzed using experimental simulations. Different types of artificial roughness, such as delta-winglet-vortex generators, ribs, or a combination of ribs and delta-winglet, were tested in a single-pass solar air heater. The objective of this study is to identify the optimal design that maximizes the thermal efficiency of a solar air heater. The relative roughness height-ratio remains constant at 0.6, although the pitch ratio is fixed at 10 and various attack angles are used. The experimental investigation was conducted within a range of Reynolds numbers (5000-14000). The usual levels of irradiance varied as 330 W/m^2 - 850 W/m^2. Based on the results, the average bulk temperature of the roughened solar air heater was 37% greater than that of a smooth SAH under peak sun irradiation. The inclined ribs at a 60° angle exhibited superior thermal efficiency compared to the other instances. These ribs covered a greater surface area and greatly enhanced the convective heat-transfer rate.

Cite this article as: Bader NM, Mushatet KS. An experimental study for a single-pass solar air heater integrated with artificial roughness. J Ther Eng 2024;10(5):1292−1305.

INTRODUCTION

The burning of-fuels and the subsequent emission of greenhouse gases are primarily responsible for global-warming, air pollution, and other associated issues. These factors have the potential to cause severe climatic disruptions and pose a significant threat to human well-being. An important challenge that the future generation will face is finding sustainable solutions to meet the growing human need for heating, cooling, and electricity. An viable substitute for conventional power plants involves harnessing renewable energy as solar, wind, wave, and among-other instances. Solar energy is a prominent kind of renewable resources derived from the reflected sun-light and heat.

A fundamental solar-air heater, which is the solar thermal systems component, may be used to harvest sunlight. The process involves absorbing thermal energy from the sun's rays and transferring it to the air in motion, so raising its temperature. Solar-heated air may be used for several purposes, including drying clothes, crops, and timber, as well as pre-heating ventilation-makeup air, among others.

*Corresponding author.
*E-mail address: amasf79@gmail.com, nabaa.m@utq.edu.iq, nabaa.m.badr@nust.edu.iq

This paper was recommended for publication in revised form by Editor-in-Chief Ahmet Selim Dalkılıç

Published by Yıldız Technical University Press, İstanbul, Turkey

Solar heaters are highly efficient and cost-effective solar thermal devices because to their simplicity and ability to utilize an abundant supply of air over a human timeframe. Enhancing the thermal efficiency of solar air heaters may help mitigate the cost effects associated with their use. To decrease heat loss in these systems, it is beneficial to produce turbulence in the fluid input by using techniques such as deploying vortex generators, ribs, or a combination of both, which also increase roughness [1-3].

Scientists used several tactics to enhance effectiveness of solar heaters, resulting in a significant shift in their study patterns. In their study, Taslim et al. [4]-tested the heat transmission in a ribbed-square channel using a liquid crystal approach. They investigated three distinct ratios of rib height to channel hydraulic-diameter (0.083, 0.125, and 0.167). Additionally, they maintained a constant ratio of rib pitch to hydraulic-diameter at 10. The researchers observed that the Nu can be enhanced by increasing the e/H ratio, with the optimal e/H ratio being between the range of 0.083 to 0.125. Thianpong et al. [5] investigated the thermal characteristics of isosceles triangular ribs that were connected to two opposite walls of a duct with an aspect ratio (AR) of 10. The researchers determined that the most efficient thermal-performance of staggered ribs may occur at a ratio of e/H equal 0.1 , P/H equal 1.0. In their study on heat-transfer rate in SAH, Nidhul et al. [6] concluded that approach fins, ribs denotes the implementation of a passive technique was the most effective. Studies on the exergetic performance of various rib designs indicate that including more ribs enhances-efficiency by (12-31.6)%, respectively, in comparison-to V-rib.

Bezbaruah et al. [7] tested the effects of SAH equipped with altered conical vortex generators arranged in a staggered pattern. They resulted in a remarkable enhancement in thermal-efficiency, with a 257% increase. The thermo-hydraulic performance parameter achieved a value of 2.04, indicating its superior performance. Mushatet and Nashee [8, 9] have shown that discrete ribs, when properly built, provide superior heat transmission on the duct wall compared to continuous-ribs CR. It was shown that, among the CR exhibit the lowest performance factor when compared to intermittent-continuous-intermittent ribs. Conversely, ribs that occurred at irregular intervals had larger friction factor values.

Further, Mushatet and Edan [10] examined the internal structure of a rectangular channel using arrays of winglet vortex generators and other geometric arrangements, such as rectangle, , triangular, semi-circle, and parabolic shapes. The heat is created on the lower surface, which may be adjusted to modify the attack angle (0° - 60°). The study showed that the suggested arrangement of vortex generators, known as common flow-up, enhances thermal efficiency and heat transfer by 170%, 240%, respectively. Kumar and Layek [11] aimed to enhance the thermal efficiency of SAH by using liquid crystal thermography. They developed an advanced SAH design including a winglet-type roughened surface. The experimental results were improved (17% - 46%) under the given circumstances. Rajendran et al. [12] conducted an experiment to assess the effectiveness of SAHs by including winglets and baffles on the surface of collector. During the testing day, a SAH with inclined baffles had an average efficiency of 52.7%, a SAH with winglets had an average efficiency of 72.9% and the flat surface SAH had an average efficiency of just 30.8%.

Furthermore, Bader and Mushatet [13] conducted experimental research using a solar simulation system to investigate the effects of combining parallel ribs with delta-winglet DWVG in SAH. The addition of combination ribs and winglets (CSAH) increased the SAH efficiency was 21.2% when compared to a smooth. In addition, Mushatet and Bader [14] assessed the solar drier thermal efficiency that has a series of DWVG. The research examined 8- pairs of DWVGs and (e/H) ratios, which varied (0.2 - 0.6). The research results indicate that the roughned solar drier, with a (e/H) was 0.6, exhibited an enhancement of roughly 6.5% in thermal efficiency and 9.4% in useable thermal energy, as compared to a smooth solar dryer.

Hajabdollahi [15] proposed a novel configuration that integrated a liquid solar collector with a fin. An efficiency of 0.6359 showed to be attainable for the optimal heat transfer rate. The air-water mass flow-rate ratio increases for heat rates ranging (0-60 kW). In their study, Chamoli et al. [16] evaluated the thermal characteristics and flow of a swept-aileron hinge SAH combined with a winglet-vortex generator. The results indicate that the winglet vortex generator with a chord-to-arc ratio at 0 and an angle ß at 30° provides the best range of total energy flux (TEF) between 1.72 and 2.20. However, the high values of the (Nu) and the (*f*) are seen at an angle (ß) at 60° and (c/a) of 1. The friction loss and convective heat transfer enhancement characteristics for airflow were assessed by Zhao et al. [17]. The DWVG, when combined with 60° V-shaped continuous ribs has the highest heat transfer performance, surpassing the case of using just WVG by 39.4%.

Rout et al. [18, 19] numerically estimated the wall temperature of an integrally finned tube for different combinations of fin number, fin height, and fin shape. Once the fin height surpasses a particular threshold, it ceases to have any impact on the wall temperature. It has been found that the mean temperature of the top surface of a horizontal tube is higher than that of the bottom layer in a situation of mixed flow. When examining the impact of various fin forms on heat transmission, it was discovered that triangular fins exhibited the lowest wall temperature. Rout et al. [20] have created an altered vapor absorption refrigerator that can maintain a chilly temperature for a whole day without the need for storage or a cold fluid. In their study, Rout et al. [21] performed an experiment to examine the effects of a hemispherical barrier on SAH. The study's results indicate that the addition of hemispherical fins to absorbent plates resulted in an important boost in efficiency.

Previous studies on roughened SAH has only explored a limited range of their possible performance qualities, based on the authors' understanding, there has been a scarcity of study on the combination of delta-winglet vortex generators with ribs. The current study examines the heat transfer enhancement in a SAH by the integration of transverse ribs (TR), inclined ribs (IR), delta-winglet vortex generators (DWVG), and a combined roughness (CSAH) individually. The delta-winglets are positioned on top of the absorber plate in their deployed state. The structure is organized in a similar flow-down pattern, with a pitch-ratio (P/e) is 10 and a relative roughness height (e/H) isf 0.6 each of the ribs and the winglets. The solar simulation system is used to heat SAH, with the hourly sun irradiation ranging (330 – 850) W/m^2, while the Reynold number is adjusted between 5000 and 14000.

EXPEEERIMENTATION

A solar simulators test system has constructed to evaluate the performance of a solar air heater collector. The system includes an absorbent plate with various artificial roughnesses. Figure 1 shows a photograph of the experimental design, while Figure 2 provides a schematic representation.

The main components of the solar simulator system, as shown in Figure 3, are halogen lights, a glass top cover, a solar-powered air duct with diameters of (1250, 360, and 50) mm, respectively, and a roughness absorber plate. Additionally, there is a solar heater. The absorber plate was heated using six halogen lamps, each having a power rating of 500 watts. During the experiment, the solar heater was setup at an angle of 31.054°, which closely resembled the tilt of Nassriya city. The optimal distance between the halogen bulbs and the covering of glass was found to be 150 mm in order to get the most precise measurement of solar irradiation.

The main objective of the paper is to examine and assess the impacts of inclined ribs (IR) at various attack angles, ranging (from 30° to 45° to 60° to 90°). In the first example, the ribs have diameters of 360 mm, 20 mm, and 30 mm, with an area of 600 mm2. In the second scenario, a total of 8-delta-winglet vortex generators (DWVG) were arranged in pairs, with each pair positioned at a 60° attack angle (ß) and a 10 mm gap between the tips of the delta-winglets (δ). The DWVG measurements are (50 length - 30 height) mm. The third case (CASH) combines transverse ribs (IR 90°) with delta-winglet vortex generators (DWVG). The roughness was affixed to an absorber plate, positioned 150 mm away from the plate edge. The winglet pairs are equipped with seven ribs that are positioned transversely at a 90º attack angle (α) with respect to the main flow. The pitch ratio, expressed as p/e, had a value of 10, while the corresponding roughness height, indicated by e/H, was 0.6. These are also pigmented with a black thermal colorant, as seen in Figure 4.

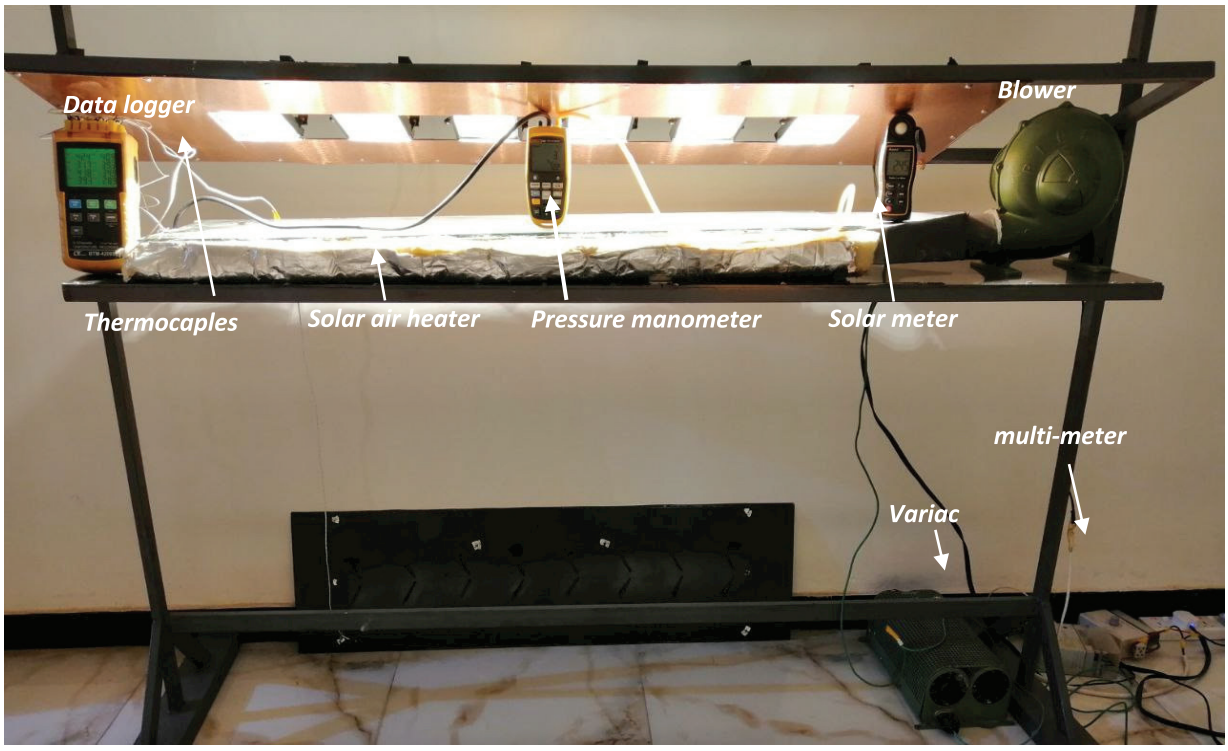

Figure 1. Photograph depicting the test equipment from an experimental perspective.

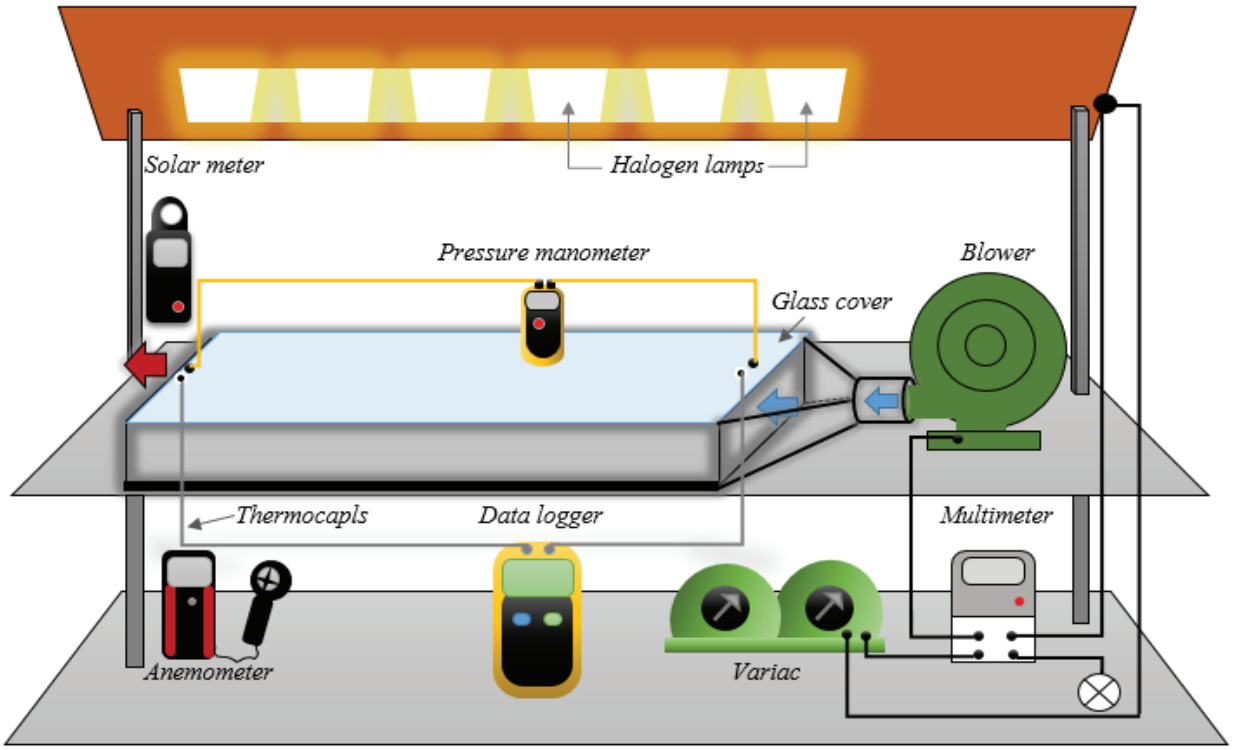

Figure 2. Illustration depicting the structural layout of the experimental perspective.

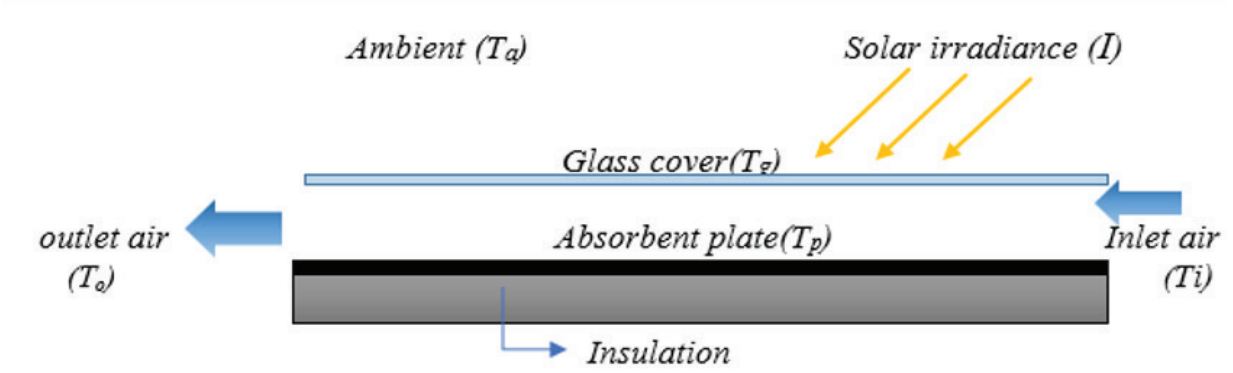

Figure 3. Single pass SAH.

A total of thirteen T-type the thermocouples were used throughout the course of this investigation. Thermocouples were furthermore positioned in different places. Figure 5 illustrates the placement of ten thermocouples that are on the down surface of the absorbent plate. These the thermocouples are arranged in four longitudinal lines, with spacing of (12, 40.5, 80.5, and 115) cm from the entrance edge. In addition, a temperature sensor was inserted inside the glass protect, while two sensors were positioned at the entrance and exit of the duct. The T-type temperature sensors are linked to a validated digital information logger kind in order to capture temperature readings. Prior to installation, all the thermocouples underwent calibration and testing.

Experimental Procedure

The variables recorded on basis 8AM - 4PM which include solar irradiation, MFR, T_o, ambient temperature, and down plate temperature at various pre-determined positions. An air blower, specifically a 3" type operating at a speed of 2800-3000 RPM, is used to facilitate the circulation of air into the heater. A stable mass flow rate (MFR) was achieved by using a blower speed controller in order

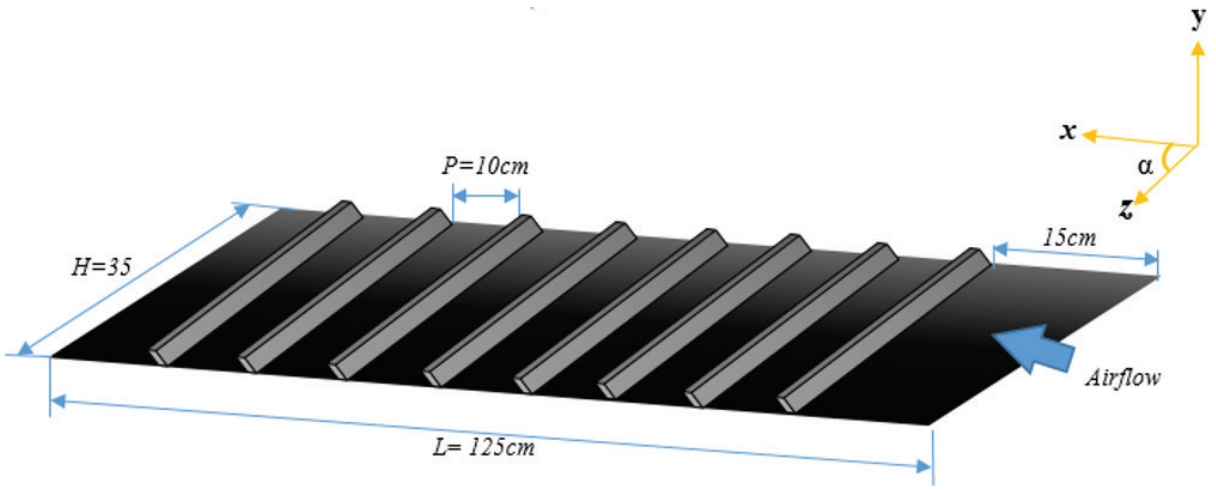

a. TR

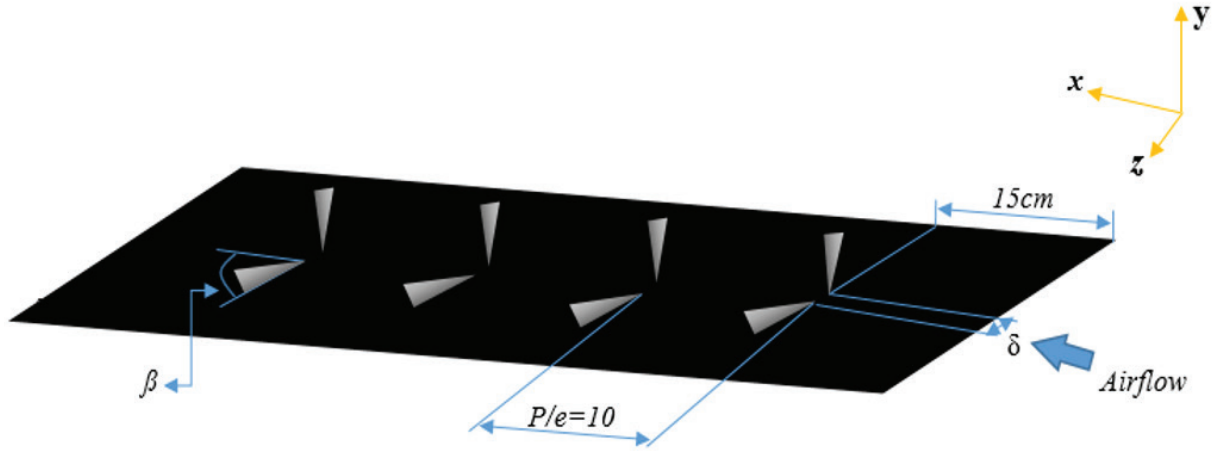

b. DWVG

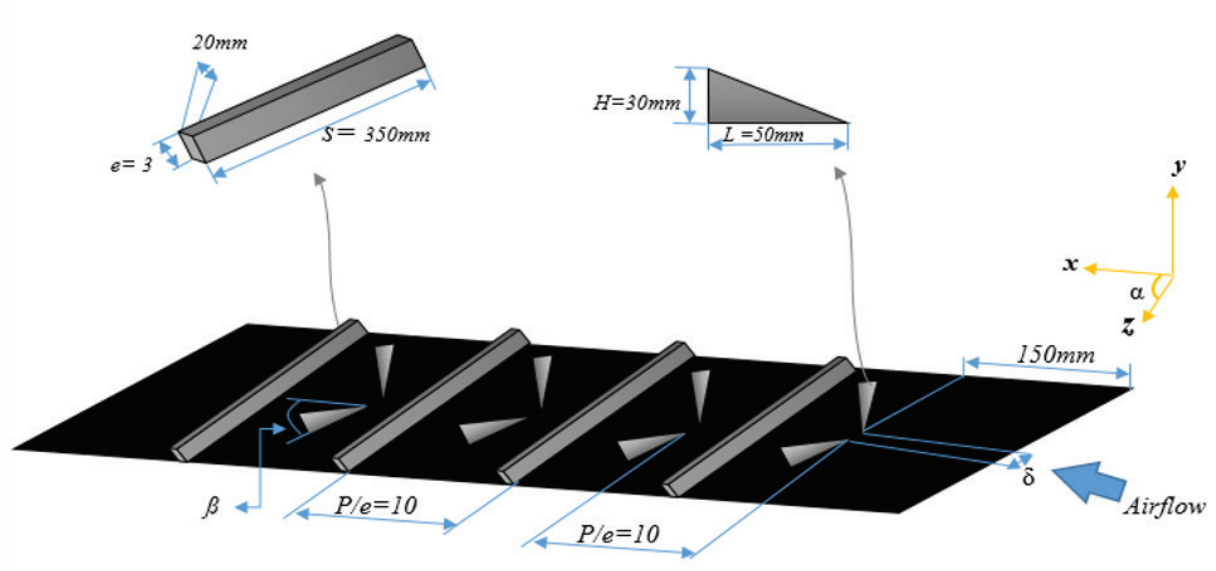

c. CSAH

Figure 4. (a), (b), and (c). The arrangement of artificial roughness cases for SAH.

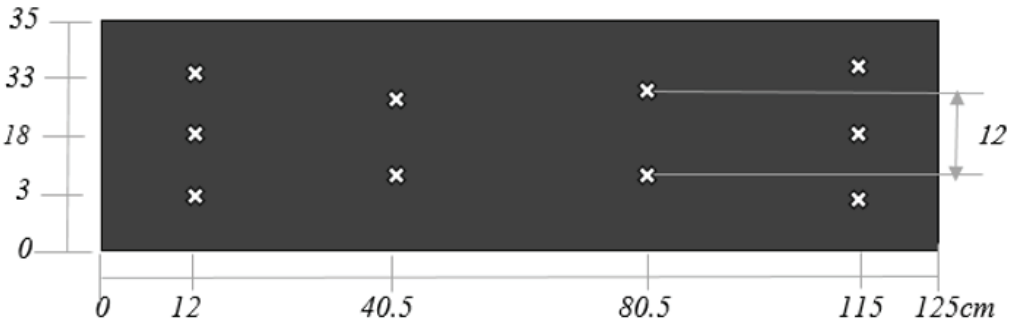

Figure 5. Schematic depicting the arrangement of thermocouples on the absorbent plate.

to manage the velocity of the flow. The halogen lights were activated and their irradiance strength was regulated by using a variac in order to align the radiation with the real sun irradiance.

The SAH performance is evaluated using 4-different absorbent plate configurations: a smooth plate, an absorbent plate with DWVG, with TR, and with CSAH. An investigation was conducted to assess the effects of including winglets and ribs on the performance of the SAH, while maintaining MFR at 0.022 kg/s. The temperature readings are shown by connecting these sensors to a data logger with an accuracy of (±0.4%+1°C) and a range of -50 to +999.9°C. The Fluke 922 airflow model is a digital pressure manometer that accurately measures the variation in static pressure throughout the duct, with a precision of (±1% + 1 Pascal). A precise digital anemometer with an accuracy of ±3% +0.5 is used for measuring air velocity. The measurement of the sunlight's intensity is determined using a A SWAR. An electrical multi-meter is a device used to accurately monitor the electrical energy consumption of an electrically powered equipment, including its frequency, voltage, and current. The kilowatt [kWh] is the standard unit of measurement for consumption of electricity on meters. It represents the amount of energy used by a one-kilowatt load over the course of one hour.

Experimental Data Reduction

The continuing research aims to determine the features of Reynolds number, turbulent airflows, and the Nusselt number. These characteristics are derived from several factors. The study included monitoring the behavior of the working fluid as it flowed with turbulence through a rectangular conduit, which was subjected to different amounts of sun irradiation. This part evaluates the fundamental equations necessary for calculating the variables.

$$\dot{m} = \rho_a U_m A_c \tag{1}$$

The calculation of the thermal efficiency SAH necessitates using of the following formula:

$$\eta = \frac{Q_u}{\mathrm{I}\ A_{\mathrm{sur}}} \tag{2}$$

$$A_{sur} = \mathrm{L\,W} \tag{3}$$

$$Q_{\mathrm{u}} = \dot{m}\, C_{\mathrm{p}} (T_{\mathrm{o}} - T_{\mathrm{i}}) \tag{4}$$

The coefficient of heat transfer may be determined using this equation:

$$h = \frac{Q_u}{A_{sur}\,(T_o - T_i)} \tag{5}$$

When the temperature of the absorbent plate is attained by:

$$T_p = \frac{1}{n}\,(\Sigma T_{pi}) \tag{6}$$

The attainment of the mean bulk temperature is accomplished by the following methods:

$$T_b = \frac{(T_o + T_i)}{2} \tag{7}$$

Below is a preliminary approximation of the Nusselt:

$$N_u = \frac{h\, D_h}{k} \tag{8}$$

The diameter of the hydraulic system is created by:

$$D_h = \frac{4A_c}{p} \tag{9}$$

$$p = 2(W + H) \tag{10}$$

$$A_c = W\, H \tag{11}$$

The friction factor may be defined using the Darcy equation as:

$$f = \frac{2\,\Delta P\;\; D_h}{L\;\rho\;U_{avrg}^2} \tag{12}$$

One way to determine the thermal effectiveness is by:

$$€ = \frac{Q_u - q_m}{\mathrm{I}\;\; A_{\mathrm{sur}}} \tag{13}$$

one obtains mechanical energy via:

$$q_m = \frac{\Delta \mathrm{P}\;\; \dot{\mathrm{m}}}{\rho_a} \tag{14}$$

The overall performance factor, which is determined as:

$$¥ = \frac{(Nu/Nu_o)}{(f\;/f_o)^{1/3}} \tag{15}$$

Uncertainty

The experimental study has undergone a three-fold test to validate the accuracy of the results. This test was conducted under similar circumstances to determine the ($T_{o)}$ and (η)for CSAH at 0.022 kg/s and a solar intensity at 850 W/m^2. The discrepancy among the 3-tests was within a range at ±0.56% in efficiency value. The outlet air temperature has a tolerance at ±2.29°C, the MFR has a tolerance at ±0.15 kg/s, and the solar intensity has a tolerance ±3 W/m^2. Determined the uncertainty using the following:

The mean, $\overline{X}_{mean}$ [8]

$$\overline{X}_{mean} = \overline{X}_{average} = \frac{\sum_1^n X_i}{n} \tag{16}$$

X_i the value of measurement. The standard deviation representation is denoted by:

$$\sigma = \sqrt{\frac{\sum_1^n (X_i - \overline{X})^2}{n-1}} \tag{17}$$

$$\sigma_m = \frac{\sigma}{\sqrt{n}} \tag{18}$$

$$x = \bar{x} \pm \sigma_m = \bar{x} \pm \frac{\sigma}{\sqrt{n}} \tag{19}$$

Theoretical Analysis

This section covers the theoretical analysis for total solar irradiance (G_T). The angular connection between any surface and the beam radiation line is the most important barrier that must be traversed to achieve a successful solar collecting procedure. Several angles affected the estimation of beam radiation. The site (Nassriya) for the trials is at 31.0538°. Users may get the declination for the days' number in a year (n) by using the equation below [22]:

$$\delta = 23.45\ sin\ (360\ \frac{284+\mathrm{n}}{365}) \tag{20}$$

The calculation of azimuth and sun angles may be performed using the following formulas:

$$\sin(\gamma s) = \frac{\cos\delta \sin\omega}{\cos\Psi} \tag{21}$$

$$\sin\Psi = \cos\varphi\cos\delta\cos\omega + \sin\varphi\sin\delta \tag{22}$$

Here is the formula to compute the incidence angle:

$$\cos\theta = \cos\Psi\cos(\gamma s)\sin\beta + \sin\Psi\cos\beta \tag{23}$$

The following statement describes a technique for calculating the average beam irradiation (G_{bn}) on a clear day: [23, 24]

$$\mathrm{G_{bn}} = A\,/e^{\mathrm{B}/\sin\Psi} \tag{24}$$

Using the incidence angle (θ), which is given by, one may approximate the beam radiation component, G_b:

$$\mathrm{G_b} = \mathrm{G}_{bn}\cos\theta \tag{25}$$

Obtain the diffuse radiation using the following formula: [25]

$$\mathrm{G}_d = \mathrm{G}_{bn}\,\mathrm{C}\,\mathrm{F}_{ss} \tag{26}$$

$$\mathrm{F_{ss}} = (1+\cos\beta)\,/2 \tag{27}$$

A formula for the foreground's ground-reflected radiation (G_r) is given by:

$$\mathrm{G}_r = \mathrm{G}_h\,\mathrm{R}\,\mathrm{F}_{sg} \tag{28}$$

$$\mathrm{G}_h = \mathrm{G}_{bn}\,(\mathrm{C} + \sin\Psi) \tag{29}$$

The angle coefficient may be determined using the following formula (F_{sg}):

$$F_{sg} = (1-cos\beta)\,/2 \tag{30}$$

The total solar radiation (G_T) given by:

$$\mathrm{G}_T = \mathrm{G}_b + \mathrm{G}_d + \mathrm{G}_r \tag{31}$$

RESULTS AND DISCUSSION

An assessment has been conducted on the ability to transfer heat of a solar collector equipped with absorber plates that have been intentionally made rough. A few consecutive unclouded days in January offered optimal circumstances for the experiments. The sun sunlight and ambient temperature are measured at one-hour periodically during daytime and then inputted into the solar simulation systems. The focus of this study was on sunlight, and thermal efficiency.

Figure 6 presents the experimental and theoretical measurements of the hourly solar intensity on January 23. The measurements were taken at the highest and lowest air ambient temperatures, which varied between 3°C and 13°C. The solar intensity radiation has a maximum point with a relative fluctuation that does not surpass 10.6%. The intensity of solar radiation gradually rises throughout the early hours of the day, peaking at midday, and then gradually decreases. The variance exhibited a curvilinear pattern, peaking around 1 PM and thereafter declining. It has been seen that the theoretical calculations surpass the experimental measurements. The scattering of radiation intensity, which may be responsible for these disparities, might be attributed to factors such as dust, fog, or other conditions that cause a portion of the incoming radiation to be reflected.

Figure 7 shows the MFR effect on thermal efficiency for smooth SAH with hourly sun irradiances varying from 5000 to 14000 at a Reynold's number. Typically, thermal

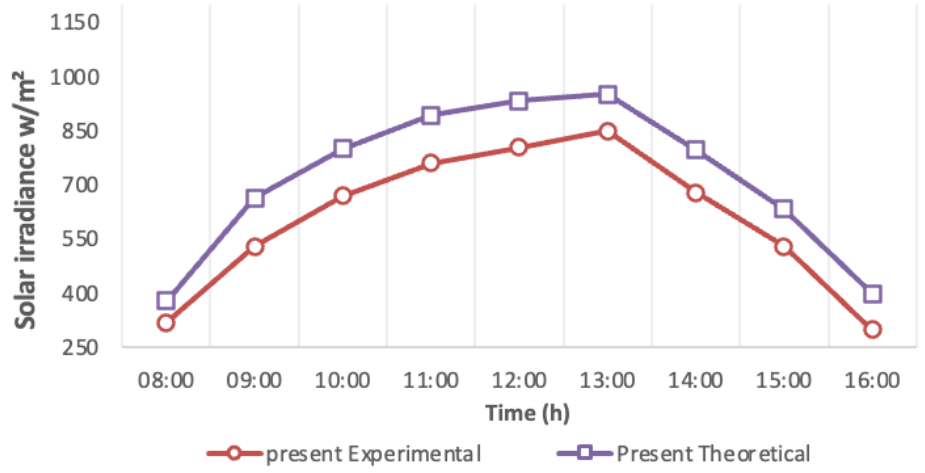

Figure 6. The experimental and numerical results comparison for solar intensity in local time.

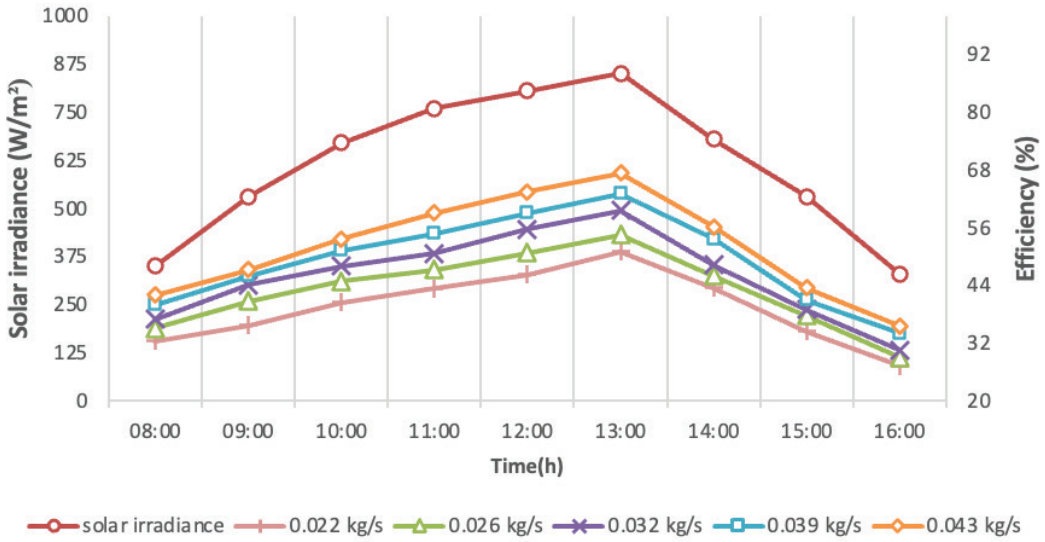

Figure 7. Hourly thermal efficiency variation for smooth SAH at various MFRs.

efficiency is shown to increase with rising sun irradiation up until around midday, when it starts to decline. It has also been shown that when MFR rises, thermal efficiency peaks. This may be due to mechanical energy superiority, which is required to overcome the friction resistance effects in the duct, or the fact that a drop in the differential temperature results in a decrease in acquired air sensible heat.

Figure 8 shows the time-dependent impact of rib attack angles on thermal efficiency at 0.022 kg/s. According to the data, there is a consistent pattern in the thermal efficiency change as a function of varying hourly sun irradiation in January for certain DWVG parameter values. The evidence is shown that ribs considerably boost thermal enhancement when compared to a smooth duct. This improvement is discernible for all targeted rib assault angles. Once the thermal efficiency reaches its maximum at 1 PM in response to increasing sun irradiation, it begins to decline. Among the several situations studied, IR 60° showed the most efficiency, demonstrating this improvement. In comparison to a smooth ductile structure, it has improved by (22%) overall. Compared to the angle of TR (IR 90°), inclined ribs (30°, 45°, and 60°) improved by (2.3, 7.7, and 9.7)%, respectively. Figure shows that decreasing the angle generated by the ribs increases thermal efficiency estimates. Since adding the ribs produces secondary flow, the inclined ribs outperform the transverse ribs in terms of heat transfer rate. The rib's existence causes local wall turbulence, which in turn disturbs the viscosity sub-layer and causes this variation. There is a difference between this and the mainstream flow, which causes a decrease in the heat transfer rate by increasing the fluid temperature locally. If the ribs are angled, the vortices will travel down the rib and mix with the main stream. So, the fluid is enter at the leading edge and leaves near the following one. As these whirls move, the leading edge of the plate comes into touch with the cold air, increasing the heat rate. However, close to the subsequent edge, there is a noticeable decrease in the heat transmission rate.

Figure 9 demonstrates the influence of TR, DWVG, CSAH and absorber plate on the thermal efficiency at a Reynolds number at 5000. The data gathered indicates a consistent pattern in the fluctuation of thermal efficiency with varying hourly sun irradiation throughout the month of January. At first, the thermal efficiency improves as the sun irradiation rises, reaching its highest point at 1 PM in a semi-linear pattern. After that, it begins to decline. It had shown that the efficiency is higher at (11.5%) for bigger ratios of DWVG compared to a smooth. The introduction of DWVGs leads to the creation of longitudinal vortices, which disturb the establishment of the boundary layer, resulting in enhanced thermal efficiency. Actually, when the flow is disrupted and mixed, it will change the original flow and temperature pattern. This will cause a delay in the point of separation of the flow and the formation of a recirculation zone in the streamlined arrangement. It enhances the blending of airflow, enabling prolonged interaction between hot and cold fluids via longitudinal vortexes. Furthermore, the turbulence level is also evident in the flow pattern inside the duct. Consequently, the rate of heat transfer increases. The TR is enhanced by (16.5%) and the CSAH is improved by (21.2%) when compartion to a flat surface.

The rib is the site of the separationi, and this layer progressively thickens as it moves upstream. Following its passage through the reattachment point, the boundary layer

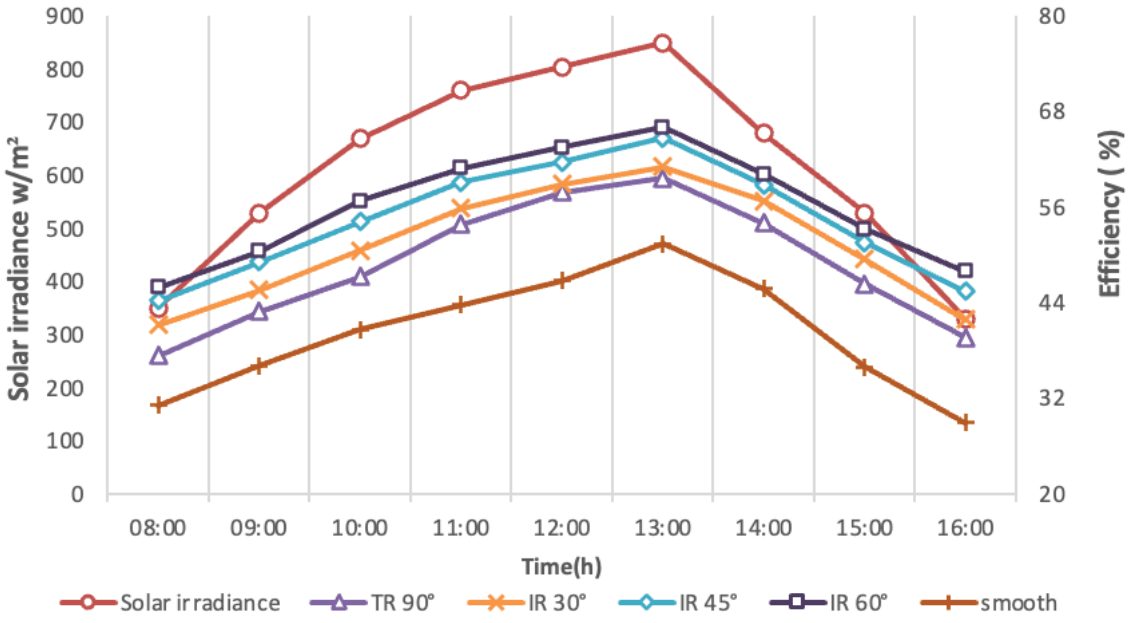

Figure 8. Hourly thermal efficiency variation at different attack angles of ribs.

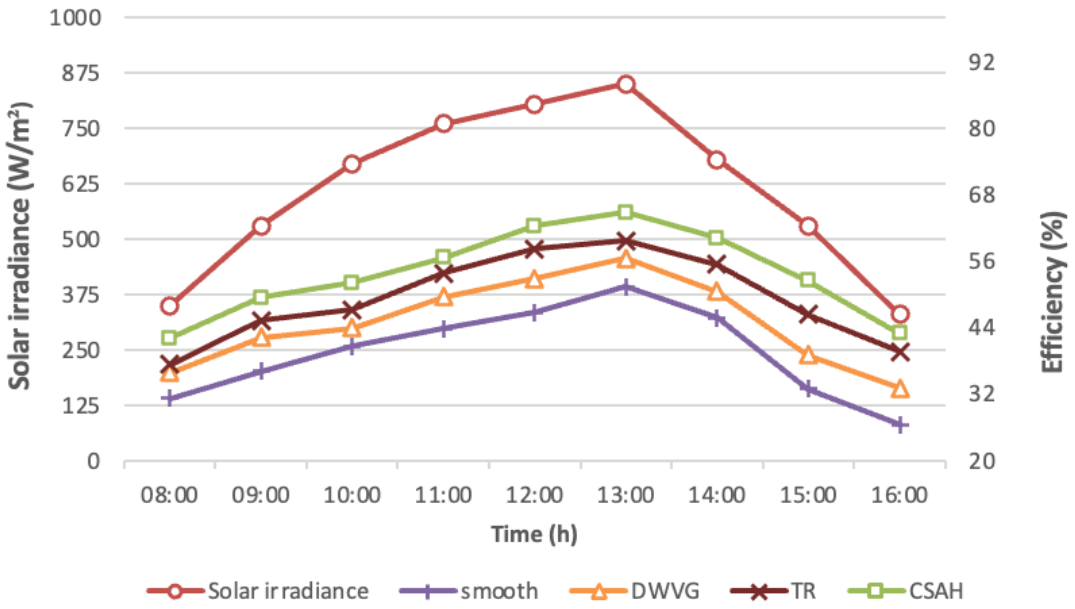

Figure 9. Hourly thermal efficiency variation for smooth and roughened SAH.

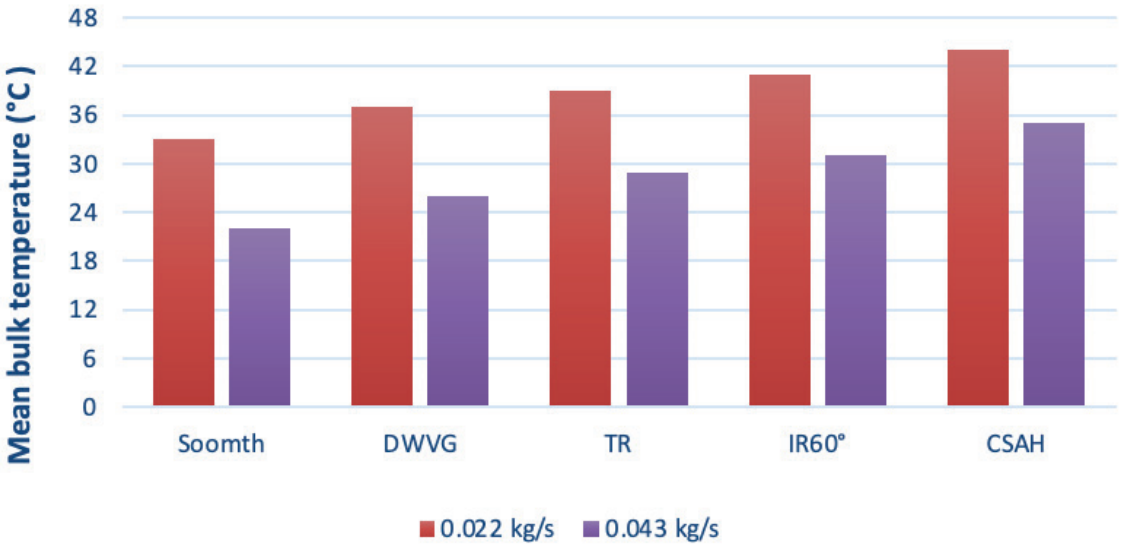

Figure 10. Comparison of mean bulk temperature for roughened and smooth SAH.

undergoes a process of self-redevelopment. The highest level of heat transmission takes place in the vicinity of a reattachment point. The combination of longitudinal swirls and transverse vortices facilitates prolonged interaction between hot and cold fluids.

For an MFR at 0.022 & 0.042 kg/s, Figure 10 compares the mean bulk temperature for the smooth, DWVG, TR, IR 60°, and CSAH. The results demonstrate that mean bulk temperature values varied considerably among situations and that MFR and mean bulk temperature have an inverse association. The data showed that the CSAH had a 37% greater increase in mean temperature values, at 0.022 kg/s, than the smooth. The presence of the winglet promotes dynamic range astute movement, which in turn increases mixing and recirculation, which in turn causes the mean temperature to rise. Causes stream mixing in the fundamental and division zones by generating longitudinal vortices with the duct flow aligned with the transverse ribs. An exponential rise in the rate of heat transfer occurs when the range-wise speed approaches the dividing surfaces.

Auxiliary counter-rotating vortices draw in cold liquid and draw warm liquid out of the divider's surface. That CSAH, winglets, and transverse ribs are more beneficial for heat transmission than a smooth protective duct plate is shown here.

This research considers all pressure losses, represented by the symbol (ΔP), which consist of losses resulting from the friction (f) generated by artificial roughness. The instance of CSAH has the highest friction values, whilst the DWVG exhibits the lowest friction factor. Furthermore, the variation in the friction is seen in relation to the Re of ducts that had equipped with different configurations of roughness. An empirical observation has shown that increasing the Re leads to a decrease in f. The relationship between the Reynolds and the friction in a range (5000-14000) is seen in Figure 11.

Take the opportunity at Figure 12, which compares the thermal efficacy of SAHs with different roughened geometries. The CSAH outperformed all of the other roughness components tested in terms of increased efficiency around the 14000 Re. Observation of this is possible. These numbers suggest that given certain values of the roughness parameters, the Re may achieve a comparable trend in effective change. The effective value grows in direct proportion to the value of Re. Perhaps this is because mechanical work accounts for the vast majority of the required effort to overcome the duct's frictional resistance. One possible explanation for this effect is because the duct's friction loss grows very little at lower Re. This might also be a possible reason for the impact. Meanwhile, due to the increase in turbulence around the roughened plate, the heat transfer amplified by the surface is rather large.

The findings are validated in Nu for asmooth solar air heater since these numerical results are then used to indicate improvements in heat transfer using CSAH. As shown in Figure 13, experimentally computed Nu are compared

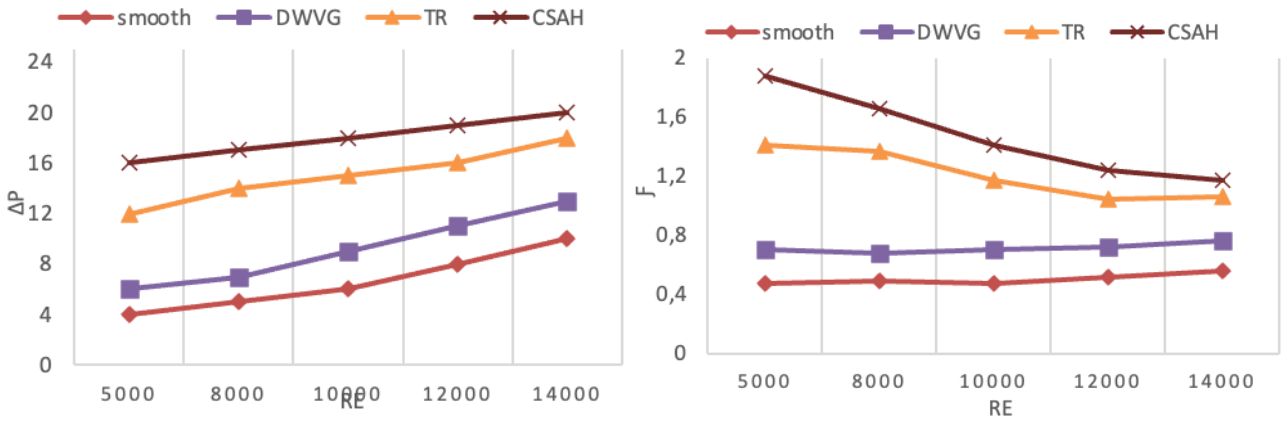

Figure 11. Pressure drop & friction factor variation for roughened and smooth SAH with Reynolds number.

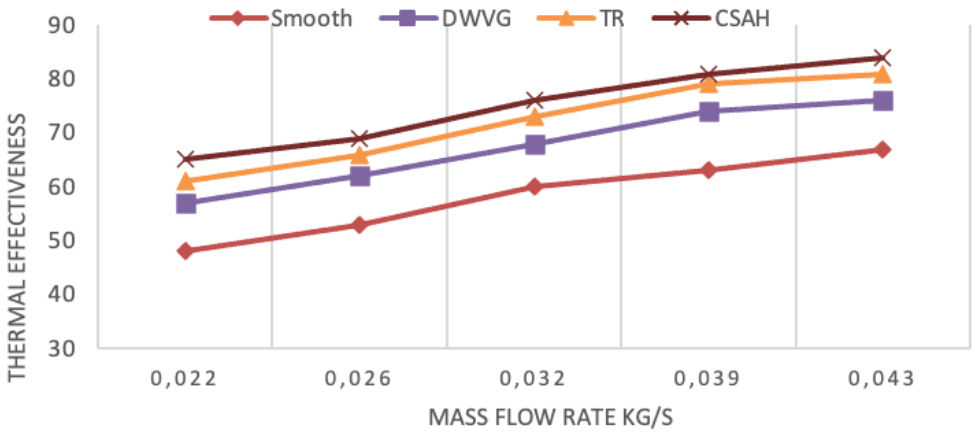

Figure 12. Thermal effectiveness for smooth and roughened SAH verse Reynolds number.

to those derived using the Dittus–Boelter equation {Nu = 0.023 $Re^{0.8}$ $Pr^{0.4}$} for 5000≤ Re ≤14000 and the data from Chamoli et al. [16]. The average absolute deviation of the numerical values around 7.2% by using the Dittus–Boelter equation. Nu deviates 8.3% between the present data for those of Chamoli et al. [16] and a smooth duct. This validation shows that the current forecasts are reasonable.

In Figure 14, we can see a comparison of the efficiency of inclined ribs in our study and in the work of Ebrahim et al. [26]. Both sets of parameters have the same α (30°-90°)and pitch ratio (10), but our height ratio was 0.034, Re ranges from 2500 to 18000, and our ribs are designed in a continuous V shape. Additionally, this study's results were compared in a study by Sivakandhan et al. [27]. Their investigation used slanted ribs with the following parameters: I (500-1000) W/m^2, MFR (0.02-0.045) kg/s, a relative angle of 1, and a relative roughness pitch differential parameter ranging from 4 to 16.

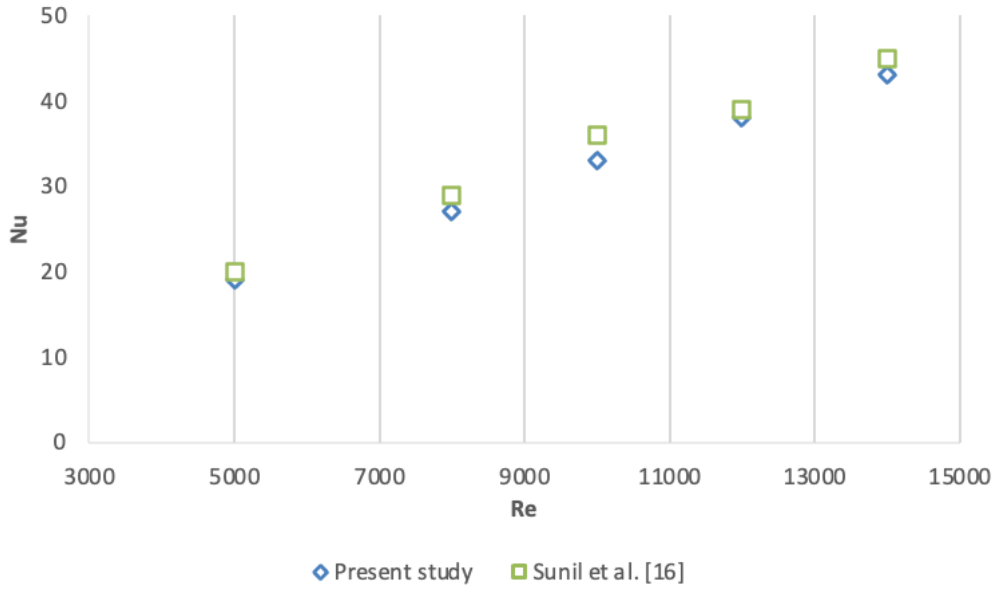

Figure 13. Comparison Nu of the smooth solar air heater.

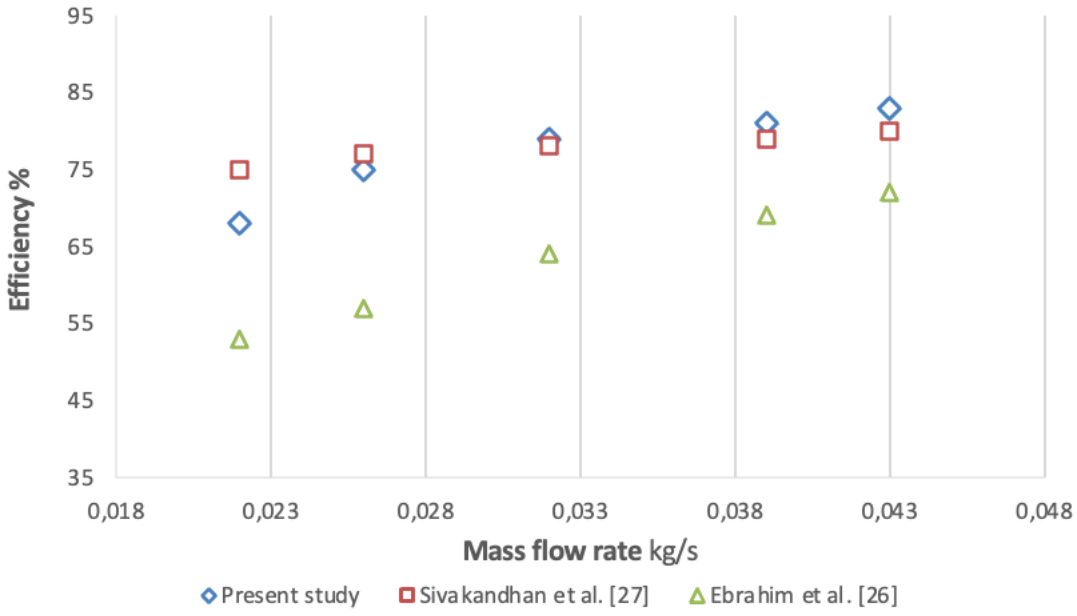

Figure 14. The ribs efficiency comparison between the present study and other research.

CONCLUSION

An experimental investigation has conducted to analyze the influence of artificial roughned on single-pass surface air heat exchangers (SAH). The solar intensity was generated using a solar simulation that replicated the meteorological conditions in January. The intensity varied on an hourly basis, ranging from 330 to 850 W/m^2. Below is a concise summary of the main findings:

- Combination (CSAH) outperformed smooth SAHs in terms of thermal efficiency by 21.2%.
- In terms of heat transfer rate performance, IR outperforms TR.
- At a Re = 5000 and maximum irradiance, the situation with IR 60° showed the highest efficiency, increased by around 10% overall in comparison to IR 90°.
- The data showed that the CSAH had a 37% greater increase in mean bulk temperature values, at 0.022 kg/s, in comparison to the smooth SAH.
- The relative variances of (Nu/Nu$_o$) ratio results for a pair DWVG do not appear to exceed 3% compared to the previous research [16].

NOMENCLATURE

A_{sur}	Absorber plate area, (m^2).
A_c	Cross-section area, (m^2).
C_p	Specific heat capacity, (J/kg. K)
H	Height of duct, (m).
I	Solar irradiance (W/m^2).
k	Thermal conductivity, (W/m. K).
L	Length of duct, (m).
Nu	Nusselt Number.
Nu_o	Nusselt number of smooth duct.
p	Perimeter of the duct, (m).
T_i	Inlet temperature, (°C).
T_o	Outlet temperature, (°C).
T_a	Ambient temperature, (°C).
T_b	Mean bulk temperature, (°C).
T_p	Absorbent plate temperature, (°C)
q_m	Mechanical energy, (J/s)
W	Width of duct, (m)
U_m	Average velocity, (m/s).
e/H	Relative roughness height.

Abbreviations

CSAH	Combined solar air heater.
DWVG	Delta-winglet vortex generator.
MFR	Mass flow rate.
SAH	Solar air heater.
TR	Transverse ribs.
IR	Inclined ribs.

Greek symbols

η	Thermal efficiency.
ρ	Fluid density at 25°C, (kg/ m^3).
δ	The gap between winglet tip, (m).
ß	Winglet angle of attack, (degree).
f	Friction factor.
ΔP	Pressure drop.
€	Thermal effectiveness.
¥	Overall performance.

AUTHORSHIP CONTRIBUTIONS

Authors equally contributed to this work.

DATA AVAILABILITY STATEMENT

The authors confirm that the data that supports the findings of this study are available within the article. Raw data that support the finding of this study are available from the corresponding author, upon reasonable request.

CONFLICT OF INTEREST

The author declared no potential conflicts of interest with respect to the research, authorship, and/or publication of this article.

ETHICS

There are no ethical issues with the publication of this manuscript.

REFERENCES

[1] Raitila J, Tsupari E. Feasibility of solar-enhanced drying of woody biomass. Bioenerg Res 2019;13:210-221. [CrossRef]

[2] Chemkhi S, Zagrouba F, Bellagi A. Drying of agricultural crops by solar energy. Desalination 2004;168:101-109. [CrossRef]

[3] Jamali B, Rasekh M, Jamadi F, Gandomkar R, Makiabadi F. Using PSO-GA algorithm for training artificial neural network to forecast solar space heating system parameters. Appl Therm Engineer 2019;147:647-660. [CrossRef]

[4] Taslim ME, Li T, Kercher DM. Experimental heat transfer and friction in channels roughened with angled, V-shaped, and discrete ribs on two opposite walls. ASME J Turbomach 1996;118:20-28. [CrossRef]

[5] Thianpong C, Chompookham T, Skullong S, Promvonge P. Thermal characterization of turbulent flow in a channel with isosceles triangular ribs. Int Comm Heat Mass Transf 2009;36:712-717. [CrossRef]

[6] Nidhul K, Yadav AK, Anish S, Kumar S. Critical review of ribbed solar air heater and performance evaluation of various V-rib configuration. Renew Sustain Energy Rev 2021;142:110871. [CrossRef]

[7] Bezbaruah PJ, Das RS, Sarkar BK. Experimental and numerical analysis of solar air heater accoutered with modified conical vortex generators in a staggered fashion. Renew Energy 2021;180:109-131. [CrossRef]

[8] Mushatet K, Nashee S. Experimental and computational investigation for 3-D duct flow with modified arrangement ribs turbulators. Therm Sci 2021;25:1653-1663. [CrossRef]
[9] Nashee SR, Mushatet KS. 3D numerical and experimental analysis for turbulent flow and heat transfer in a duct integrated with ribs turbulators. TEST Engineer Manage 2020;83:21810-21821.
[10] Mushatet KS, Edan IL. Effect of winglet vortex generators orientation on heat transfer enhancement. Int J Mech Mechatron Engineer 2018;18:8-24.
[11] Kumar A, Layek A. Evaluation of the performance analysis of an improved solar air heater with Winglet shaped ribs. Exp Heat Transf 2022;35:239-257. [CrossRef]
[12] Rajendran V, Singaraj K, Rajarathinam J. Environmental, economic, and performance assessment of solar air heater with inclined and winglet baffle. Environ Sci Pollut Res Int 2023;30:14337-14352. [CrossRef]
[13] Bader NM, Mushatet KS. Thermal performance improvement of artificially roughened solar air heater. Engineer Rev 2022;43:66-81. [CrossRef]
[14] Mushatet KS, Bader NM. Experimental investigation for the performance of the solar air dryer with vortex generator. Defect Diffus Forum 2022;419:57-67. [CrossRef]
[15] Hajabdollahi H. Thermoeconomic assessment of integrated solar flat plate collector with cross flow heat exchanger as solar air heater using numerical analysis. Renew Energy 2021;168:491-504. [CrossRef]
[16] Chamoli S, Lu R, Xu D, Yu P. Thermal performance improvement of a solar air heater fitted with winglet vortex generators. Sol Energy 2018;159:966-983. [CrossRef]
[17] Zhao Z, Luo L, Qiu D, Wang Z, Sunden B. On the solar air heater thermal enhancement and flow topology using differently shaped ribs combined with delta-winglet vortex generators. Energy 2021;224:119944. [CrossRef]
[18] Rout SK, Mishra DP, Thatoi DN, Acharya AK. Numerical analysis of mixed convection through an internally finned tube. Adv Mech Engineer 2012;4:918342. [CrossRef]
[19] Rout SK, Thatoi DN, Acharya AK, Mishra DP. CFD supported performance estimation of an internally finned tube heat exchanger under mixed convection flow. Procedia Engineer 2012;38:585-597. [CrossRef]
[20] Rout SK, Pulagam MKR, Sarangi SK. Prospect of a fully solar energy-driven compact cold store for low income farming communities. In: Ramgopal M, Rout SK, Sarangi SK, eds. Advances Air Conditioning and Refrigeration Singapore: Springer; 2021. pp. 13-21. [CrossRef]
[21] Rout SK, Mohapatra T, Mohanty CP, Mishra P. Experimental investigation of thermal performance of solar air heater having hemispherical fins on absorber plates. In: Ramgopal M, Rout SK, Sarangi SK, editors. Advances Air Conditioning and Refrigeration Singapore: Springer; 2021. pp. 337-343. [CrossRef]
[22] Hannun RM, Hamoud MA. Comparison study for the utilization of solar power with different positions lie in Iraq and on the equator and northern region. Thesis, University of Thi-Qar, Iraq; 2021.
[23] Ekechukwu O, Norton B. Review of solar-energy drying systems II: An overview solar drying technology. Energy Conver Manage 1999;40:615-655. [CrossRef]
[24] Joudi KA. Some aspects of solar irradiance calculations. In: Proceedings of the 3rd Arab International Solar Energy Conference; Feb 1988; Baghdad.
[25] Ekechukwu OV, Norton B. Review of solar-energy drying systems III: Low temperature air-heating solar collectors for crop drying applications. Energy Conver Manage 1999;40:657-667. [CrossRef]
[26] Ebrahim MA, Saini JS, Solanki SC. Heat transfer and friction in solar air heater duct with V-shaped rib roughness on absorber plate. Int J Heat Mass Transf 2002;45:3383-3396. [CrossRef]
[27] Sivakandhan C, Arjunan TV, Matheswaran MM. Thermohydraulic performance enhancement of a new hybrid duct solar air heater with inclined rib roughness. Renew Energy 2020;147:2345-2357. [CrossRef]